Hindawi
Shock and Vibration
Volume 2019, Article ID 7683952, 16 pages
https://doi.org/10.1155/2019/7683952

Research Article

Nonlinear Dynamic Characteristics of Marine Rotor-Bearing System under Heaving Motion

Yongchao Han and Ming Li

Department of Mechanics, Xi'an University of Science and Technology, Xi'an, 710054 Shaanxi, China

Correspondence should be addressed to Yongchao Han; 526702348@qq.com

Received 16 August 2018; Accepted 13 December 2018; Published 14 January 2019

Academic Editor: Mario Terzo

In this paper, the influence of the heaving motion on the nonlinear dynamic behavior of the rotor-bearing system is considered. First, a mathematic model of the marine rotor-bearing system is developed on the short bearing theory in the noninertial reference system, in which the heaving motion is taken into account. Then its dynamic characteristics are analyzed based on the numerical integration method, such as the bifurcation diagram, the largest Lyapunov exponents (LLE), the steady-state response, and the rotor orbit and its Poincaré map. The results indicate that heaving motion has a great effect on the dynamics of the rotor system, which exhibits a period 1 motion at low rotating speed, with the increase of the rotating speed, the phenomena of the quasiperiodic, period 2, and double Hopf bifurcations appear. Its dynamic performance presents a period 1 motion, period 2, quasiperiodic, and chaotic oscillation.

1. Introduction

When sailing ship suffers unpredictable oceanic conditions such as sever sea condition, different travel factors such as wind and wave will drive the ship swaying, heaving, surging, rolling, pitching, and yawing at a low frequency, which are typically transport motion for rotor-bearing system. All of these forms of motion will have a serious impact on marine rotor-bearing system. The most significant impacts on the stable operation and safety of a ship are rolling, pitching, and heaving [1] during its running by various disturbances.

Generally, existing research studies about influences of transport motion on dynamics of rotor-bearing system are focused on its dynamic characteristics under maneuvering flight. Nelson and Meacham [2] established a multishaft rotor-bearing system, which contains blade loss, base shock, maneuver loads, and specified fixed frame forces. Furthermore, the research presented a method of component mode to analyze the forced response. Lin et al. [3] mainly discussed the impact of climbing angle on nonlinear dynamic response of a cracked aircraft rotor system in maneuvering flight, in which the investigation indicates that the climbing angle can make a nonnegligible difference to the dynamic parameters and stability of the rotor. Afterwards, Cho et al. [4] put forward combined analysis method to study dynamics of rotor and dynamic components of a rotorcraft. At the same time, Zheng [5] introduced a maneuver equivalent force to establish a new model to compensate for the influence of maneuvering on AMB-rotor stability. Furthermore, Hou et al. [6] also applied the multiscale method to study the superharmonic resonance response of an aircraft cracked rotor caused by maneuvering; later in reference [7], they computed its nonlinear dynamic response of aircraft rotor system by introducing the Herbst flight parameters to control maneuvering flight. Wang et al. [8] simulated the dynamic property of a rotor system under centrifugal force and base movements, which is El Centro seismic wave. And Wang et al. [9] studied the influence of gusts caused by helicopter rotors on the stability of the rotor and its dynamic behaviors.

In addition, several studies have been published on the effect of the dynamic response of ship under transport

motion. Qin et al. [10] investigated nonlinear rolling displacement of the ship considering the rolling angle and the heavy loads on deck. Soon Holden et al. [11] proposed a parametric model of roll ship, in which its dynamic characteristics is highly compatible with experimental results that have heaving and pitching motions. Simonsen et al. [12] experimented the motion of container ship in different sea situations, which are in calm water and regular head seas. Thereafter, Lee et al. [13] created a database by collecting motion data from a ship with six degrees of freedom in different ocean states. Until now, there have been few research studies on marine rotor-bearing system dynamic characteristics under transport motion especially the heaving motion. Chen et al. [14] developed a dynamic model of flexible rotor systems and designed a new test rig to simulate the effects of time-variable base motions. The result showed that the rotation of the foundation could cause the nonlinear characteristics. However Zhang et al. [15] carried out the dynamic analysis of marine rotor after thinking about the basement motion and introducing a new nonlinear oil film force model; furthermore, in reference [16], they also studied nonlinear dynamics property of marine rotor system under pitching and rolling motion. Meanwhile, Zhao et al. [17] established a mathematic model of marine rotor-bearing, in which the air bag and floating raft are embedded.

Among all the researches mentioned above, most of the literatures have paid attention to the dynamic behaviors of the rotor-bearing system with base motion or the dynamic response of the ship under wave loads. Little work has been investigated on dynamics of marine rotor-bearing system under heaving motion, which is one of the most important transport oscillations. In the present study, the nonlinear dynamic model of marine rotor system takes the motion of ship into consideration, and the dynamic characteristics are analyzed by the method of nonlinear dynamics, such as the bifurcation, the rotor orbit, and its Poincaré map.

2. Nonlinear Dynamic Model

Figure 1 shows the transport motion of a ship and a marine rotor-bearing system, in which the bearing basement and the disc are regarded as rigid bodies with mass, regardless of the movement in the z direction. The x_0 and y_0 are translational displacements of the carrier, x_1 and y_1 are the displacements of the rotor relative to the carrier, and x and y are the displacements of the rotor involved with the ship heaving. O_0-$X_0Y_0Z_0$ is a fixed reference system, O-$X_1Y_1Z_1$is the one attached to the ship, and O-XYZ is established in the rotor-bearing system.

Based on the short bearing theory, we should consider the effect of heaving motion on the system in the x direction. According to Newton's law, the rotor-bearing differential equations of motion can be expressed as

$$\begin{aligned} m\ddot{x} &= F_x[(x-x_0),(y-y_0),(\dot{x}-\dot{x}_0),(\dot{y}-\dot{y}_0)] \\ &\quad + me\omega^2\cos\omega t - m\ddot{x}_0 + mg, \\ m\ddot{y} &= F_y[(x-x_0),(y-y_0),(\dot{x}-\dot{x}_0),(\dot{y}-\dot{y}_0)] \\ &\quad + me\omega^2\sin\omega t, \end{aligned} \tag{1}$$

where m is the mass of disc; F_x and F_y are the nonlinear oil film force components in x and y directions, respectively; e is eccentricity; and ω is the speed of rotor.

2.1. Nonlinear Oil Film Force. Figure 2 illustrates schematic diagram of a journal bearing, in which F_τ and F_r are the nonlinear oil film forces in radial and tangential directions, respectively.

The nonlinear oil film forces are obtained by solving the Reynolds equation under certain assumptions. In this study, the hydrodynamic short journal bearing theory is introduced, and the Reynolds equation for oil film force p can be expressed as

$$\frac{\partial}{\partial z}\left(\frac{h^3}{\mu}\frac{\partial p}{\partial z}\right) = 6(\Omega - 2\dot{\theta})\frac{\partial h}{\partial \varphi} + 12\dot{e}\cos\varphi, \tag{2}$$

where $h = c + e\cos\theta = c(1+\varepsilon\cos\varphi)$, φ and h are circumferential azimuth and bearing oil film thickness, respectively, e is the eccentricity of the bearing, and θ is angle of the journal equilibrium position.

In view of the semi-Sommerfeld condition, which is $p|_{z=-B/2} = p|_{z=B/2} = 0$, the nonlinear oil film expressions of radial and tangential direction are obtained:

$$\begin{cases} F_\mathrm{r} = 2\mu BR\left(\dfrac{R}{c}\right)^2\left(\dfrac{B}{2R}\right)^2\left[\Omega - 2\dfrac{d\theta}{dt}G_1 + 2\dfrac{d\varepsilon}{dt}G_2\right], \\ F_\tau = 2\mu BR\left(\dfrac{R}{c}\right)^2\left(\dfrac{B}{2R}\right)^2\left[\Omega - 2\dfrac{d\theta}{dt}G_3 + 2\dfrac{d\varepsilon}{dt}G_4\right], \end{cases} \tag{3}$$

$$\begin{aligned} G_1 &= \frac{2\varepsilon^2}{(1-\varepsilon^2)^2}, \\ G_2 &= \frac{\pi(1+2\varepsilon^2)}{2(1-\varepsilon^2)^{5/2}}, \\ G_3 &= \frac{\pi\varepsilon}{2(1-\varepsilon^2)^{3/2}}, \\ G_4 &= \frac{2\varepsilon}{(1-\varepsilon^2)^2}, \end{aligned} \tag{4}$$

where c, μ, and B are the bearing clearance, lubricant film viscosity, and bearing length, respectively. ε is eccentricity of the journal. R is the bearing radius.

2.2. Nondimensional Motion Equation. In order to make the study more broadly applicable, regard the bearing clearances c and time as the basic parameters, using the dimensionless parameter expressions shown in Table 1 to nondimensionalize the equations. The dimensionless nonlinear oil film force in equation (3) expression is obtained as follows:

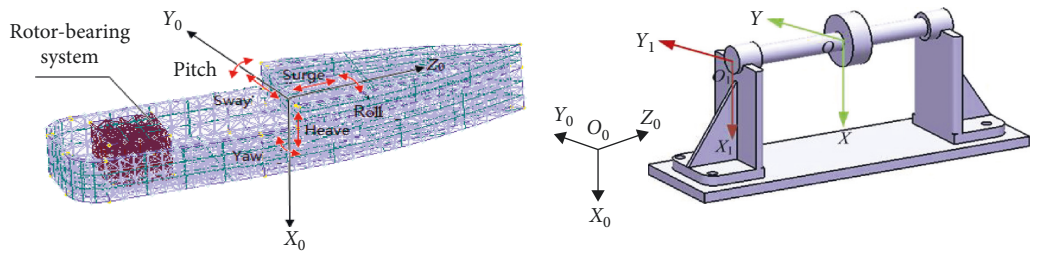

Figure 1: Schematic diagram of transport motion of ship and a marine rotor-bearing system. (a) Transport motion. (b) Rotor-bearing system.

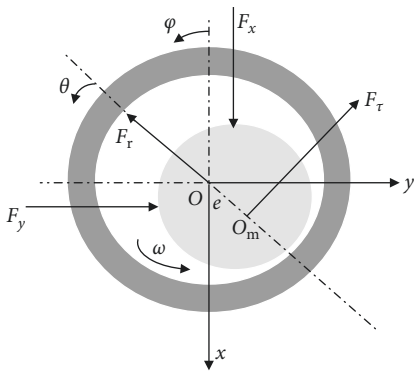

Figure 2: Schematic diagram of journal bearing.

Table 1: The expression of nondimensional parameter.

Parameter description	Expression	Dimensional unit
Nondimensional frequency ratio η	$\eta = \omega/\omega_0$	rad/s
Nondimensional time τ	$\tau = \omega t$	s
Nondimensional eccentricity α	$\alpha = e/c$	m
Nondimensional displacement of rotor X	$X = x/c$	m
Nondimensional displacement of rotor Y	$Y = y/c$	m
Nondimensional displacement of ship $^{-}X_0$	$^{-}X_0 = x_0/c$	m
Nondimensional displacement of ship $^{-}Y_0$	$^{-}Y_0 = y_0/c$	m
Nondimensional Sommerfeld number σ	$\sigma = \overline{\sigma}/m\sqrt{gc}$	Pa·s
Nondimensional speed Ω_0	$\Omega_0 = \sqrt{c\omega^2/g}$	rad/s
Nondimensional oil film force $f_{i,i=x,y}$	$f_i = F_i/mg$	N
Length-diameter ratio λ	$\lambda = B/(2R)$	m

$$\begin{cases} f_r = \dfrac{\sigma\lambda^2\omega\left[(1-2\varphi')G_1 + 2e'G_2\right]}{3}, \\ f_\tau = \dfrac{\sigma\lambda^2\omega\left[(1-2\varphi')G_3 + 2e'G_4\right]}{3}, \end{cases} \tag{5}$$

where σ is nondimensional Sommerfeld number and λ is the length-diameter ratio.

Projecting the coordinate change of equation (5) into the oxy plane, the nondimensional oil film force in the x and y directions are expressed as

$$\begin{cases} f_x[(x-x_0),(y-y_0),(\dot{x}-\dot{x}_0),(\dot{y}-\dot{y}_0)] = -f_r\cos\varphi - f_\tau\sin\varphi, \\ f_y[(x-x_0),(y-y_0),(\dot{x}-\dot{x}_0),(\dot{y}-\dot{y}_0)] = -f_r\sin\varphi + f_\tau\cos\varphi, \end{cases} \tag{6}$$

For heaving motion discussed in this paper, it is reasonable to assume that ship heaving is $X_0 = A_0\sin\omega_0 t$ based on the existing theoretical study. According to $\dot{x} = (dx/dt), \dot{y} = (dy/dt), x' = (dx/d\tau), y' = (dy/d\tau)$, the motion equation's dimensionless expression is obtained as shown below:

$$\begin{aligned} X'' &= \frac{f_x}{\Omega_0^2} + \alpha\cos\tau + \frac{A_0}{\eta^2}\sin\frac{\tau}{\eta} + \frac{1}{\Omega_0^2}, \\ Y'' &= \frac{f_y}{\Omega_0^2} + \alpha\sin\tau, \end{aligned} \tag{7}$$

where η is the nondimensional frequency ratio, A_0 is the nondimensional heaving amplitude, α is the dimensionless eccentricity, Ω_0 is the dimensionless speed, and f_x and f_y are dimensionless oil film forces in the x and y directions, respectively. From equation (7), it is obvious that the heaving motion will produce an inertial force on the system. Based on the nonlinear dynamics theory, it makes the dynamic characteristics of steady-state response more complex, which will be discussed in detail in the following section.

3. Nonlinear Dynamics Analysis

3.1. Nonlinear Dynamics of Rotor-Bearing System under Heaving Motion. For the purpose of heaving motion effect on the dynamics of the rotor-bearing system, the case was calculated when there was no heaving motion for comparative analysis.

The displacement bifurcation diagram and the largest Lyapunov exponent curve of the rotor system without heaving are shown in Figure 3(a), in which the dimensionless speed Ω_0 changes from 0.8 to 3.3, $\sigma = 3$, $\alpha = 0.1$,

and $\lambda = 0.2$. Initial conditions X, X', Y, and Y' are 0.2, 0, 0.1, and 0, respectively. At low speeds, such as Ω_0 from 0.8 to 2.1, the steady-state displacement of the rotor under the effect of eccentricity is represented by the period 1 motion with small amplitude. With the increase of rotating speed, when Ω_0 changes from 2.1 to 2.8, the rotor system appears doubling period bifurcation from period 1 to period 2 and its steady-state response suddenly increases. When the speed Ω_0 is from 2.8 to 2.95, the system transits from period 2 to period 1. While the speed Ω_0 changes from 2.95 to 3.15, the system has a transition from period 1 to quasiperiodic bifurcation; the displacement of steady-state response begins to gradually increase at this time. Along with a further increase in speed Ω_0 from 3.15 to 3.3, the system is bifurcated from quasi-periodicity into chaos, and the rotor-bearing system amplitude increases sharply right now. The figure shows the rotor system is very rich in nonlinear dynamics.

Figure 3(b) illustrates the bifurcation diagram of the displacement of the rotor and the curve of the largest Lyapunov exponent under heaving motion. It is obtained by the numerical integration method with the rotation speed Ω_0 ranging from 0.8 to 3.3, in which parameters are $\sigma = 3$, $\alpha = 0.1$, $\lambda = 0.2$, $A_0 = 110$, and $\eta = 100.58$. Initial conditions X, X', Y, and Y' are 0.2, 0, 0.1, and 0, respectively. At low speeds, such as Ω_0 from 0.8 to 2.1, the steady-state response of the rotor is a synchronous motion with small amplitude and exhibits periodic 1 characteristic. With the increase of rotational speed, the quasiperiodic bifurcation occurs when Ω_0 varies from 2.1 to 2.2, and the displacement of the rotor suddenly increases. While the speed Ω_0 varies from 2.2 to 2.5, the system from quasiperiodic bifurcation transforms to period 2. Then, the system diversifies from period 2 to quasiperiodic bifurcation when the speed Ω_0 is from 2.5 to 2.7, and double Hopf bifurcation occurs at this time which is the unique characteristics of the rotor system under the heaving motion compared with Figure 3(a). With the speed increasing further, the system is still in the quasiperiodic bifurcation stage when Ω_0 changes from 2.7 to 3.08, but the displacement of the system steady-state response goes through a gradual decrease and starts to increase. The system bifurcates from quasiperiodic motion to chaos motion at high speeds when Ω_0 varies from 3.08 to 3.3, and simultaneously the amplitude of the rotor-bearing system increases sharply. The bifurcation diagram shows a richer dynamical behavior of the rotor system under heaving conditions than without heaving.

Accordingly, it can be found that the heaving motion has a great influence on the dynamic characteristics of the system, that is, the inertial force caused by the heaving motion leads to the multifrequency vibration of the rotor system. For instance, when the rotation speed is $\Omega_0 = 1.8$ under the same conditions, the motion without heaving is in a simple period 1. Instead, under heaving motion, it is characterized by quasiperiodic motion state, in which the displacement fluctuation is larger and frequency domain response is more complex. Besides, such phenomena can be easily found by comparing Figures 3(a) and 3(b).

Figure 4 indicates the steady-state response, frequency spectrum, rotor trajectory, and Poincaré map of the rotor system, in which $\Omega_0 = 0.9$, $\eta = 100.58$, and $A_0 = 110$. It can be seen from Figure 4(b) that the frequency f_0 due to the heave is obviously the main component, which is not equal to zero. The frequency f_0 is about 0.0045. In addition to the frequency f caused by unbalanced force, its frequency multiplication components $2f$, $3f$, $4f$, etc., also appear. There is only the power frequency f and its frequency multiplication shows that the rotor is in synchronized movement characteristics. At this point, the heaving motion plays a leading role in the dynamic characteristics of the system; however, the nonlinear oil film force has no obvious effect on the dynamic characteristics of the rotor. From Figure 4(c), the rotor orbit is a regular ellipse formed by multiple coincident curves, and the periodic motion characteristics of the rotor synchronization are obvious. The Poincaré map shows an isolated periodic attractor. The largest Lyapunov exponent is −0.22498, judging the system is in period 1 state.

Figure 5 illustrates the steady-state response of the rotor when the rotation speed $\Omega_0 = 2.2$, $\eta = 100.58$, and $A_0 = 110$. The amplitude of the displacement changes is shown in Figure 5(a). f_0 caused by the heaving motion is still a significantly predominant component peak; meanwhile, frequency component f and its harmonic components $2f$, $3f$, etc., remain existing. At this moment, the combined frequency of $(f_0 + f)/2$ and its odd times component peaks obviously cannot be neglected, and the harmonics bifurcation phenomenon occurs in the doubling frequency and half-frequency components. The highlighting of the combined frequency and odd multiple components indicate that the rotor has entered a complex motion state; the heaving motion and the unbalance force as well as nonlinear oil film forces affect the rotor's dynamics. The orbit of the rotor appears as an oscillation in an irregular annular region, and there is a large curvature change of the rotor trajectory at certain positions of the ring. In the Poincaré map, there is a line and a ring formed by discrete points. The largest Lyapunov exponent of the system is −0.04014. It shows that the system is in quasiperiodic motion.

Compared with Figure 3(a), the heaving motion makes the rotation speed of the rotor system into the quasiperiodic characteristics advance by about 28%, and at the same time, the displacement of the rotor system increases by about 55%. Moreover, the combined frequency in the frequency response of the rotor system occupies a large proportion, which shows that the oil film force caused by the heave motion has an insignificant effect on the dynamic characteristics of the rotor system.

Figure 6 demonstrated the steady-state response of the rotor under the parameter of the rotation speed $\Omega_0 = 2.33$, $\eta = 100.58$, and $A_0 = 110$. The time domain response of the rotor system is shown in Figure 6(a). The frequency component f_0 caused by heaving motion is approximately equal to the power frequency component f. The power frequency's multiplication components $2f$, $3f$, and $4f$ and the odd multiple components 3 $(f_0 + f)/2$, 5 $(f_0 + f)/2$, and 7 $(f_0 + f)/2$ of the combined frequency $(f_0 + f)/2$ and so on are still there. This moment, the continuous increasing of both frequency component f_0 and combined frequency $(f_0 + f)/2$, indicates that the rotor dynamics will be more complicated. Moreover,

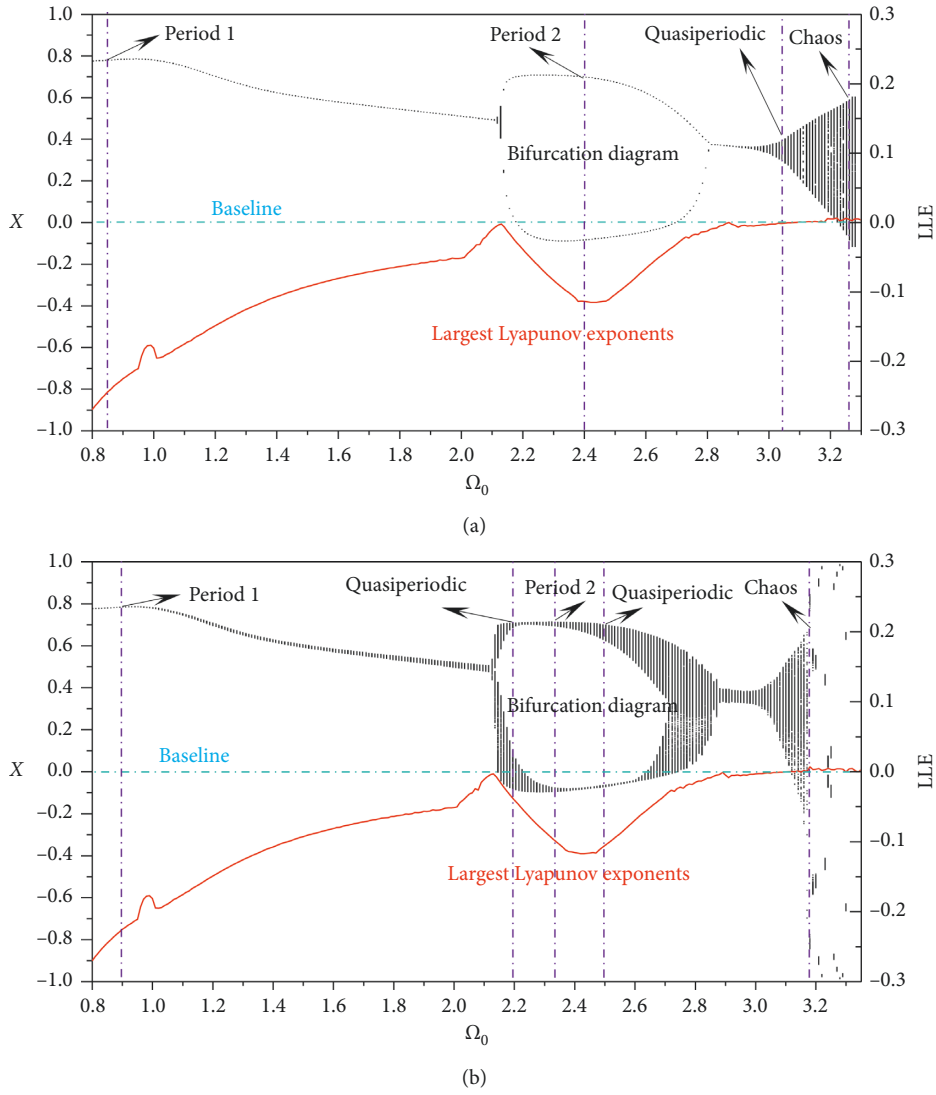

Figure 3: The bifurcation diagram of displacement X and its largest Lyapunov exponents. (a) The steady-state responses of the rotor-bearing system and its largest Lyapunov exponents without heaving. (b) The steady-state responses of the rotor-bearing system and its largest Lyapunov exponents under heaving.

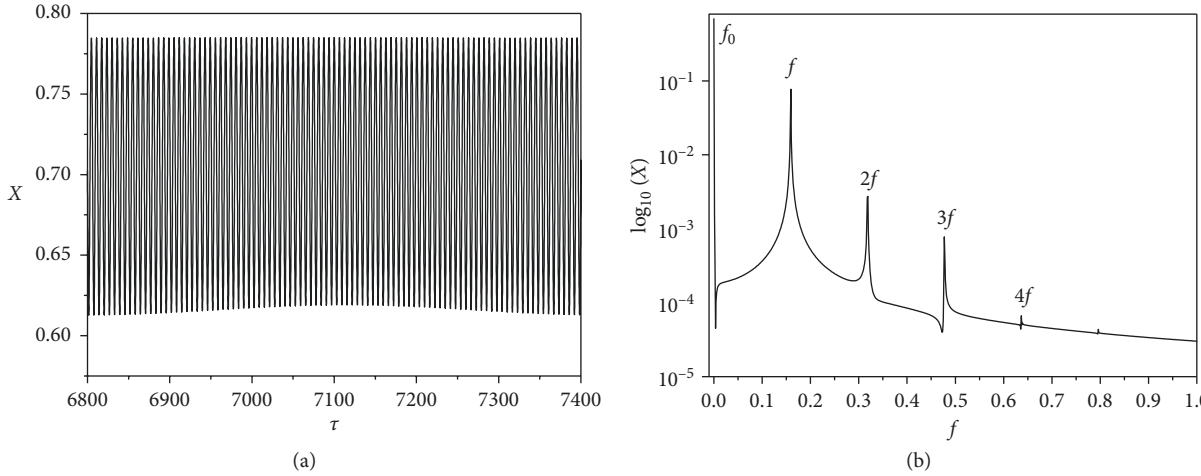

Figure 4: Continued.

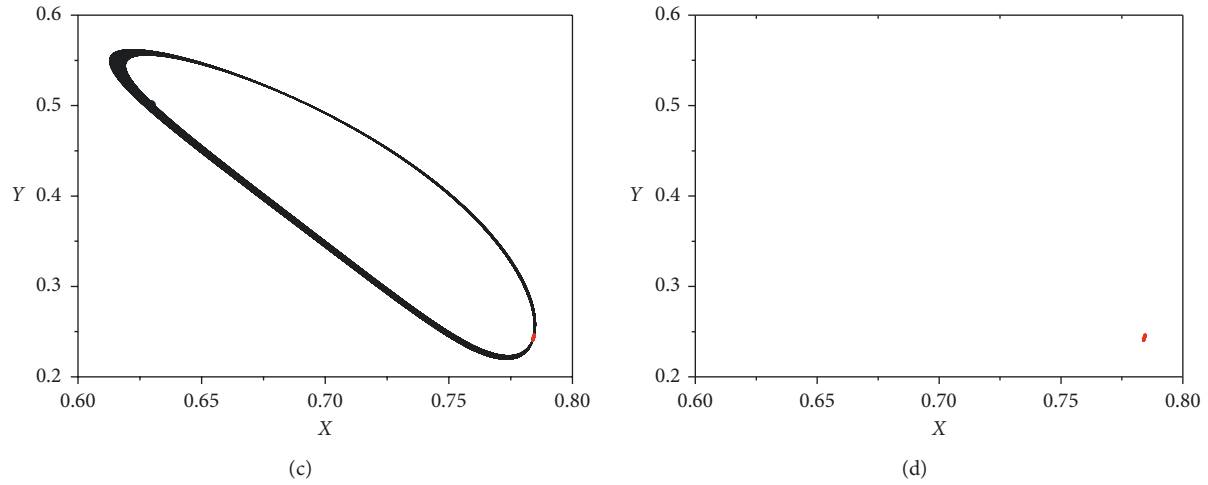

Figure 4: (a) Displacement. (b) Frequency response. (c) Rotor orbit. (d) Poincaré map where $\Omega_0 = 0.9$, $\eta = 100.58$, and $A_0 = 110$.

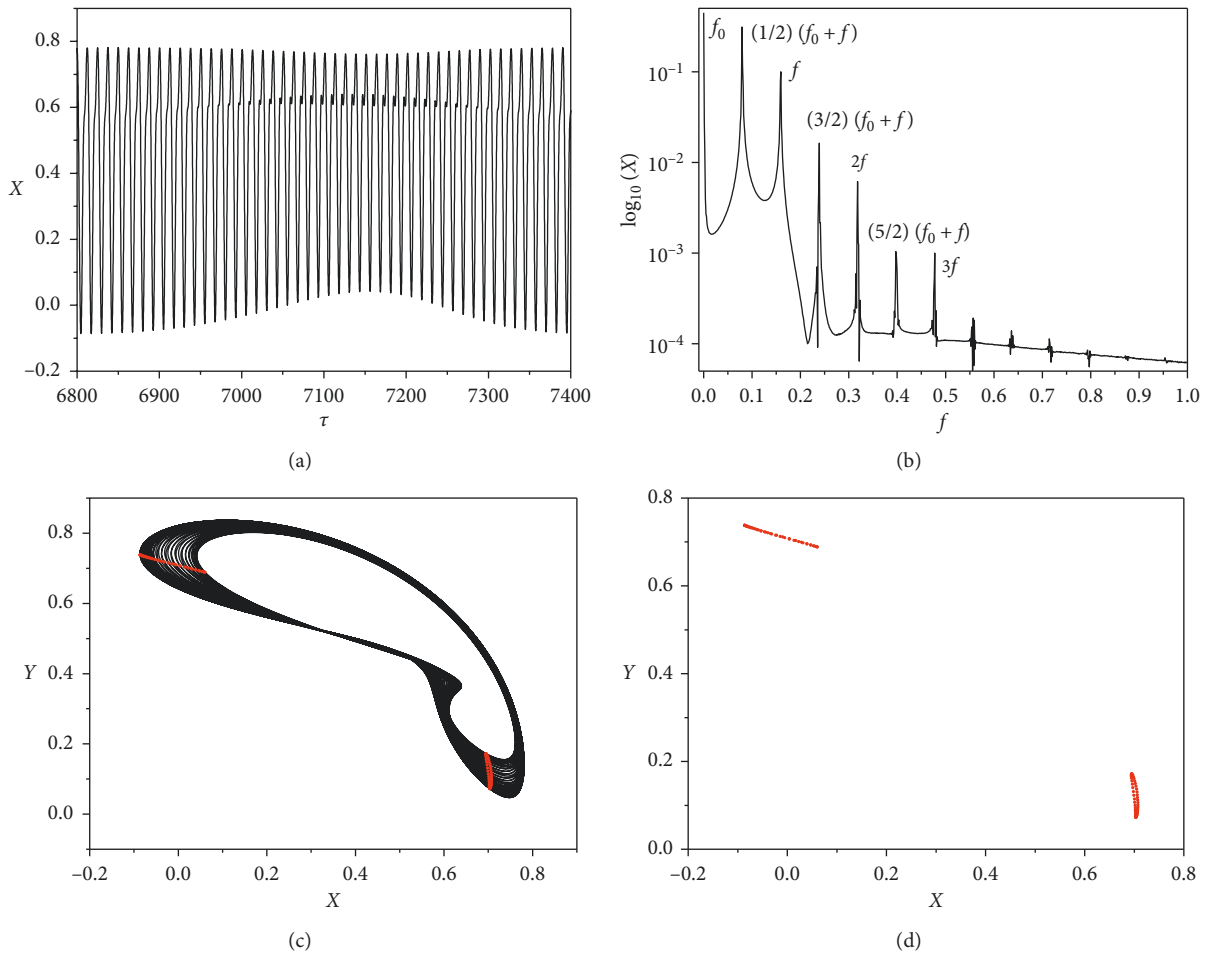

Figure 5: (a) Displacement. (b) Frequency response. (c) Rotor orbit. (d) Poincaré map where $\Omega_0 = 2.2$, $\eta = 100.58$, and $A_0 = 110$.

the increase of $(f_0 + f)/2$ also indicates the half-frequency whirl phenomenon of the oil film. As is shown in the Figure 6(c), the orbit of the rotor shows a "banana-type" trajectory, and the lower part of the trajectory shows a "band-shaped" region where the trajectory curves do not overlap. In the Poincaré map, there are two isolated periodic attractors. Compared with Figure 3(a), the rotor system has occurred double Hopf bifurcation phenomenon,

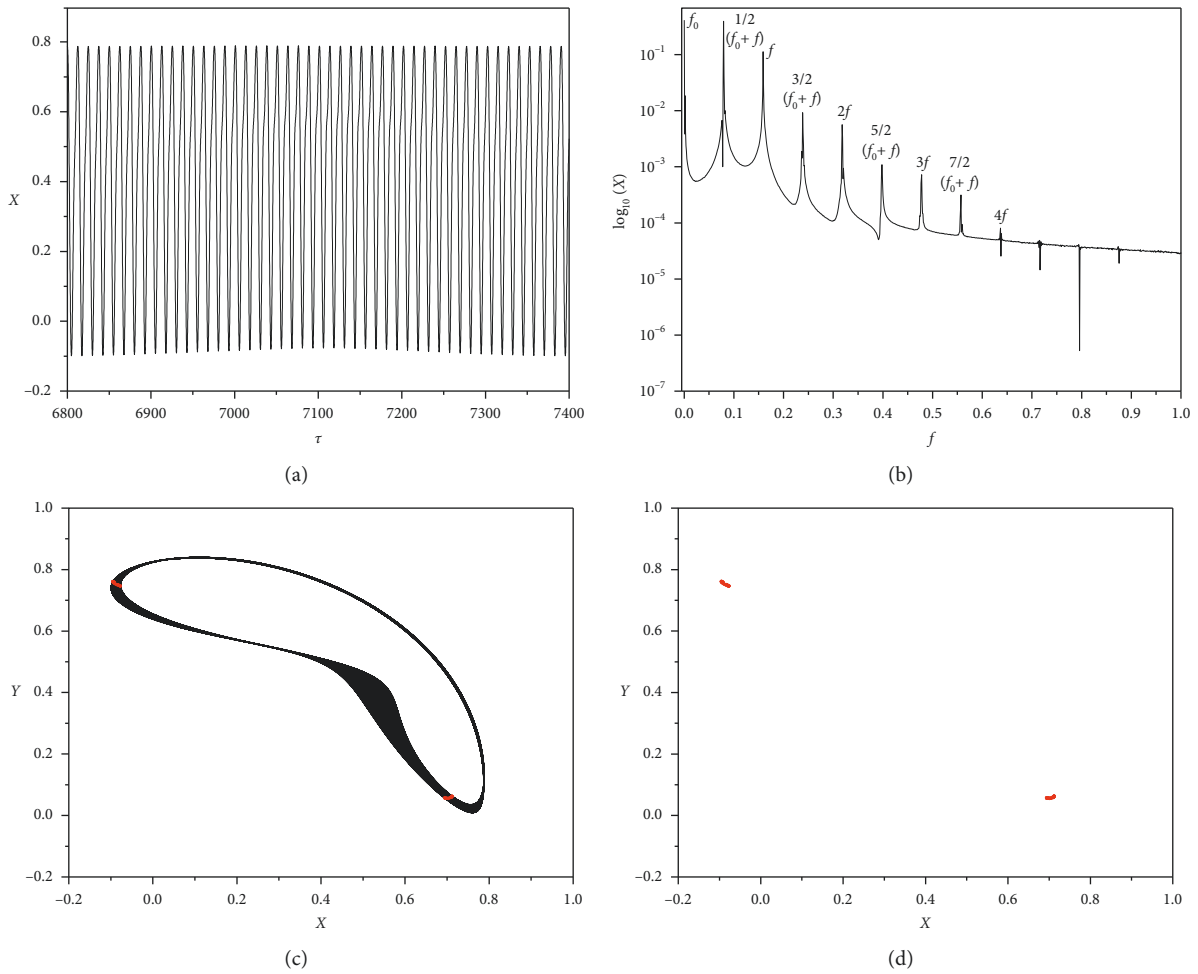

Figure 6: (a) Displacement. (b) Frequency response. (c) Rotor orbit. (d) Poincaré map where $\Omega_0 = 2.33$, $\eta = 100.58$, and $A_0 = 110$.

which, what's more, becomes more and more obvious with the rotational speed increasing Similarly, the largest Lyapunov exponent is −0.09648. The system is in period 2 movement.

Figure 7 gives the steady-state response of the rotor system when rotational speeds $\Omega_0 = 2.5$, $\eta = 100.58$, and $A_0 = 110$. Figure 7(a) shows that the rotor's displacement and amplitude tend to be stable with little change. In the Figure 7(b), there are the frequency component f_0 generated by heaving motion and the power frequency component f caused by the unbalance force. Simultaneously, the multiplication frequency $2f$, $3f$, $4f$, and $5f$ and the combined frequency $(f_0 + f)/2$ and its odd frequency multipliers 3 $(f_0 + f)/2$, 5 $(f_0 + f)/2$, 5 $(f_0 + f)/2$, 7 $(f_0 + f)/2$, 9 $(f_0 + f)/2$ coexist. The presence of harmonic components' discrete spectrum peaks indicates that the nonlinear characteristics of the oil film force on the rotor system response continue to increase. Figure 7(c) shows the rotor trajectory that in some locations no longer coincides with each other in the horizontal and vertical directions. There is a large range of "band-like" fluctuations; moreover, the "band-shaped" region tends to expand as compared with Figure 6(c). In Figure 7(d), Poincaré map illustrates an isolated point and a set of point-sets with regular "linear" distribution. In this case, Hopf bifurcation also occurs in another branch of bifurcation diagram. With the increase of rotating speed, this phenomenon will be more and more obvious; the largest Lyapunov exponent of rotor system is −0.10504; all above determine the system is quasiperiodic bifurcation.

Figure 8 displays the steady-state response of the rotor system at speeds of $\Omega_0 = 2.85$, $\eta = 100.58$, and $A_0 = 110$. Figure 8(a) shows that with the further increase of the rotation speed, the displacement amplitude of the system will have a large change and no longer be stable. At this moment, the frequency component f_0, the power frequency component f and its frequency multiplication components $2f$, $3f$, $4f$, and $5f$, and the combined frequency $(f_0 + f)/2$ and its odd multiple components 3 $(f_0 + f)/2$, 5 $(f_0 + f)/2$, 7 $(f_0 + f)/2$, and 9 $(f_0 + f)/2$ coexist. The proportion of heaving motion is significant. The harmonic components of each spectrum peak cannot be ignored; even the harmonic components show a continuously increasing trend. The effect of oil film force on the rotor system is more obvious and is more severe; in Figure 8(c), the rotor orbit is restricted to oscillate inside a cylinder and the curvature changes obviously. In the Poincaré map, the point set is arranged according to a certain rule. The largest Lyapunov exponent of the system is −0.00831, which means that the system is in the quasiperiodic stage.

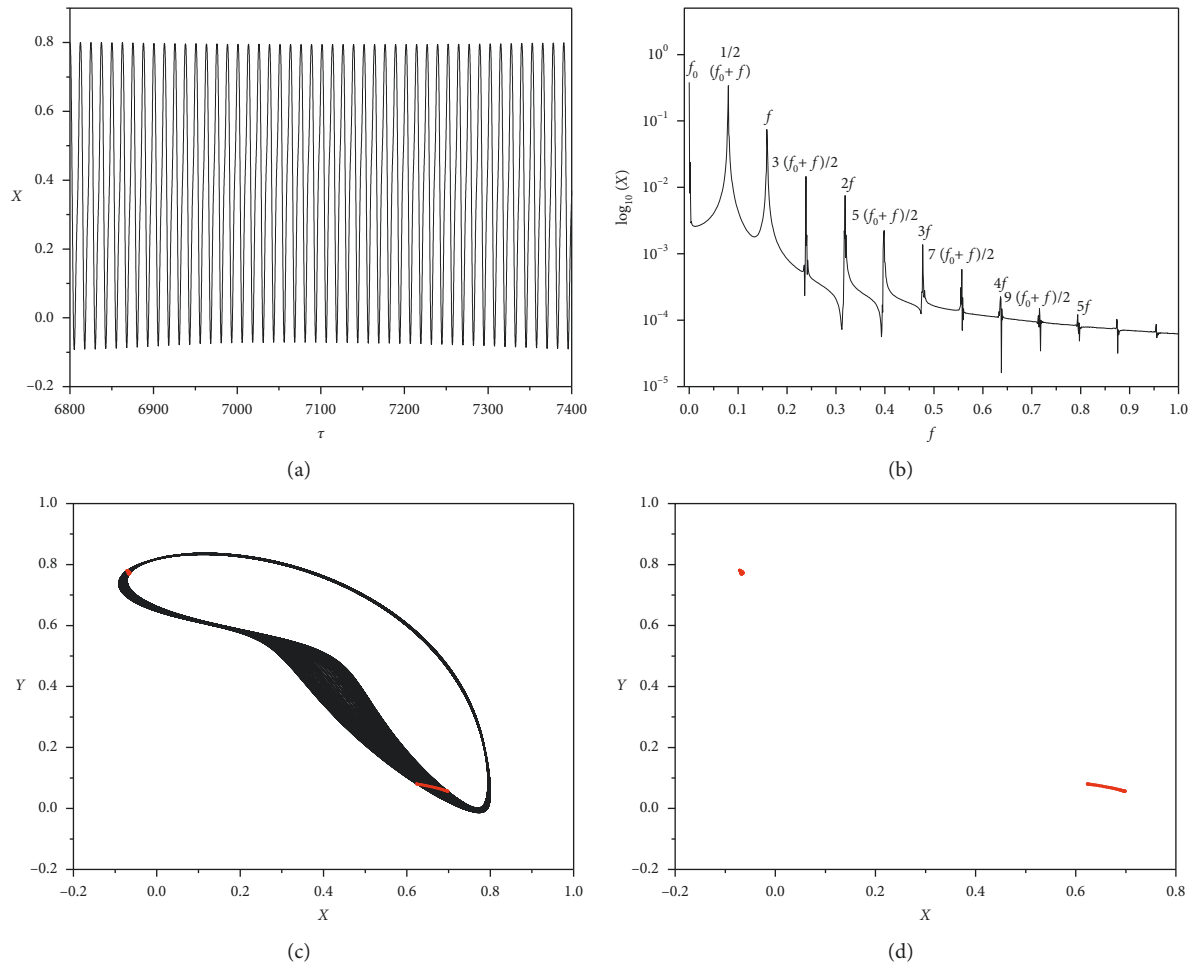

Figure 7: (a) Displacement. (b) Frequency response. (c) Rotor orbit. (d) Poincaré map where $\Omega_0 = 2.5$, $\eta = 100.58$, and $A_0 = 110$.

In contrast to Figure 3(a), the heaving motion makes the displacement amplitude of rotor increase by about 50%. In the later period of the quasiperiodic bifurcation, the influence of the heaving motion on the dynamic characteristics of the rotor system becomes more apparent. The heave motion obviously causes the nonlinear oil film force to produce continuous influence on the rotor system, thus the phenomenon of oil film whirl will be more significant.

Figure 9 demonstrates the steady-state response of the rotor system, in which the rotational speed $\Omega_0 = 3.18$, $\eta = 100.58$, and $A_0 = 110$. The increasing speed and heaving motion effect make the rotor system displacement rapidly increase and change rapidly in the direction of heaving. In the spectrum Figure 9(b), there is frequency component f_0 that is generated by heaving motion, a power frequency component f caused by unbalanced force and its frequency multiplication component $2f$. In addition, the combined frequency $(f_0 + f)/2$ and its odd-numbered multiple component $(f_0 + f)/2$ and its unconventional harmonic components are clearly highlighted. More and more harmonic components appear densely and harmonic components begin to branch, and dense spectrum peak finally forms a chaos spectrum, which indicates that the system's dynamic characteristics have entered a very complex stage. At this point, it is given from Figure 9(c) that the orbit of the rotor is confined to a disorderly and irregular oscillation in an ellipsoidal domain. A "tire" attractor appears that consists of a set of points with irregular distribution in the Poincaré map. Calculating the largest Lyapunov exponent at this speed as 0.00722, we can determine that the system is chaotic.

Compared with Figure 3(a), it can be seen that the heaving motion advances the speed of the rotor into the chaotic phase, and the rotor's motion characteristics become more complicated due to the effect of heaving. The orbit of the rotor becomes more chaotic, and the generation of wave component and combined frequency indicate that the heaving motion seriously influences the dynamic characteristics of the rotor system by the oil film force.

3.2. Parametric Analysis. Just obtaining the steady-state response of the rotor system, the analysis of the system's nonlinear dynamic behaviors is not finished because the amplitude and frequency ratio of the heaving motion will have a great influence on the dynamics of the rotor system; therefore, it is necessary to analyze the heaving parameters.

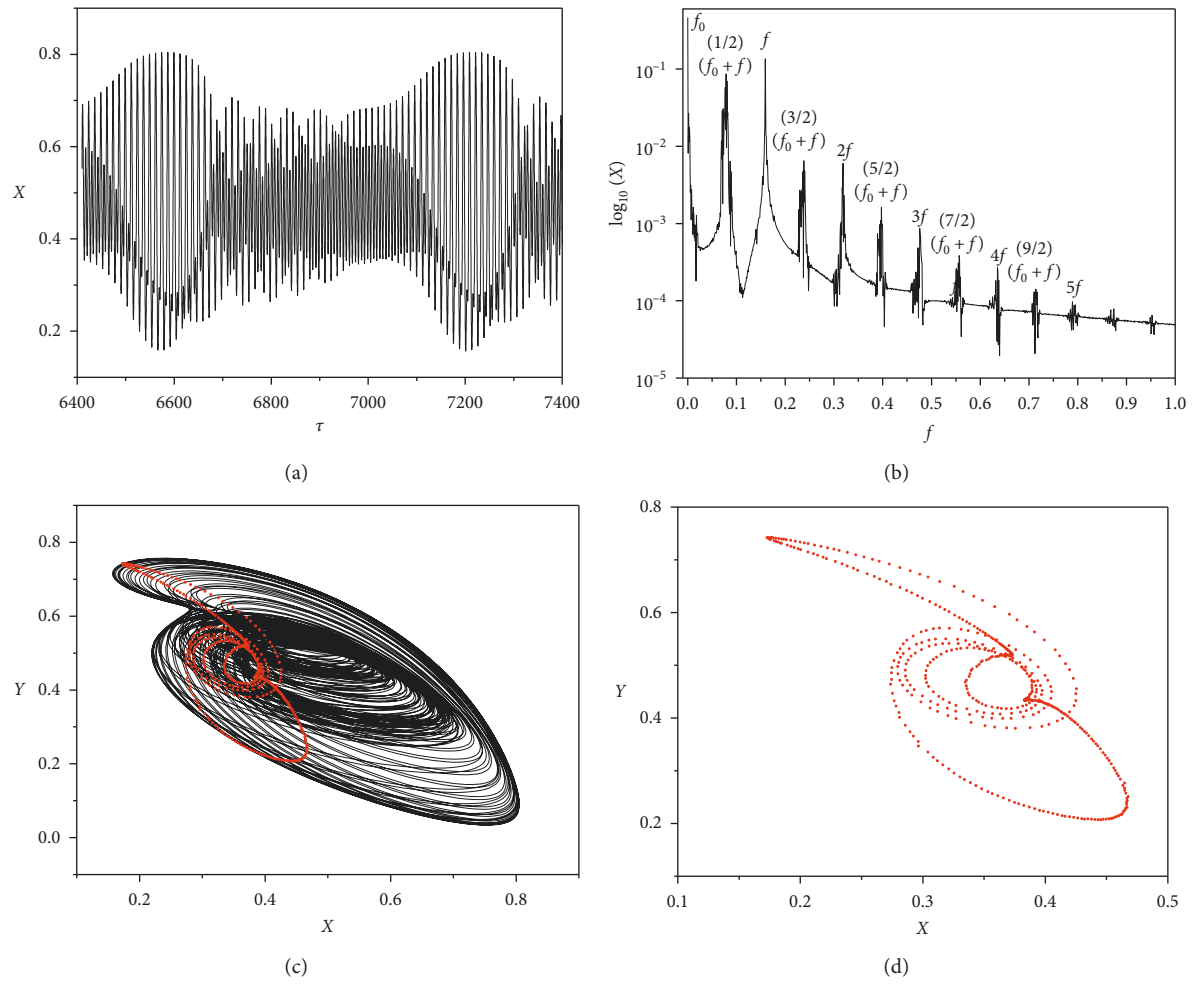

Figure 8: (a) Displacement. (b) Frequency response. (c) Rotor orbit. (d) Poincaré map where $\Omega_0 = 2.85$, $\eta = 100.58$, and $A_0 = 110$.

Figure 10 presents the displacement of the rotor with the frequency ratio changing from 25 to 200 at the speed $\Omega_0 = 2.12$, amplitude $A_0 = 110$, $\sigma = 3$, $\alpha = 0.1$, and $\lambda = 0.2$. Initial conditions X, X', Y, and Y' are 0.2, 0, 0.1, and 0, respectively. It can be obviously seen that when the frequency ratio is small such as η from 25 to 80, at the beginning, the displacement of the system is large. Then, with the increasing of the frequency ratio, the displacement gradually decreases to be stable. At this moment, the dynamic characteristics of the system are mainly affected by the influence of heaving motion and nonlinear oil film force and present chaotic motion. As the frequency ratio continues to increase, the vertical displacement of the rotor gradually increases as the frequency ratio η is 80 to 130. At this point, the continuous influence of the heaving motion causes a significant change of the oil film force having affected the rotor system, making the displacement of the rotor be no longer stable but begin to increase continuously. The rotor system exhibits a quasiperiodic motion state.

The frequency component f_0 caused by the heaving motion and the power frequency f occupies the main components in the spectrogram Figure 11(b), and at this point, a large number of continuously increasing irregular harmonic components of each frequency component in the spectrogram appear, all of which form a chaotic peak. The trajectory of rotor is disorderly, and its Poincaré map indicates a messy chaotic attractor. In summary, it can be concluded that the rotor is in chaotic state.

Figure 12 represents the steady-state response of the system where the frequency ratio = 85, $\Omega_0 = 2.12$, $\eta = 85$, and $A_0 = 110$. The displacement of the rotor decreases and tends to be stable as the frequency ratio increases. At this moment, in the frequency diagram, the power frequency f and its multiplication components $2f$, $3f$, $4f$, $5f$, etc., coexist; meanwhile, the frequency component f_0 caused by the heave does not disappear but becomes more weaker than before. Especially, the combined frequency component $(f + f_0)/2$ of the system is highlighted, and the appearance of the combined frequency indicates that the rotor system motion state will become complicated. The axis trajectory of the rotor appears as a "band" ellipse and its Poincaré map is a "band" area made up of a series of discrete points, thus the system is in a quasiperiodic motion state.

Figure 13 illustrates the dynamic response of the system with the parameters $\Omega_0 = 2.12$, $\eta = 105$, and $A_0 = 110$. The continuous increase of the frequency ratio causes the

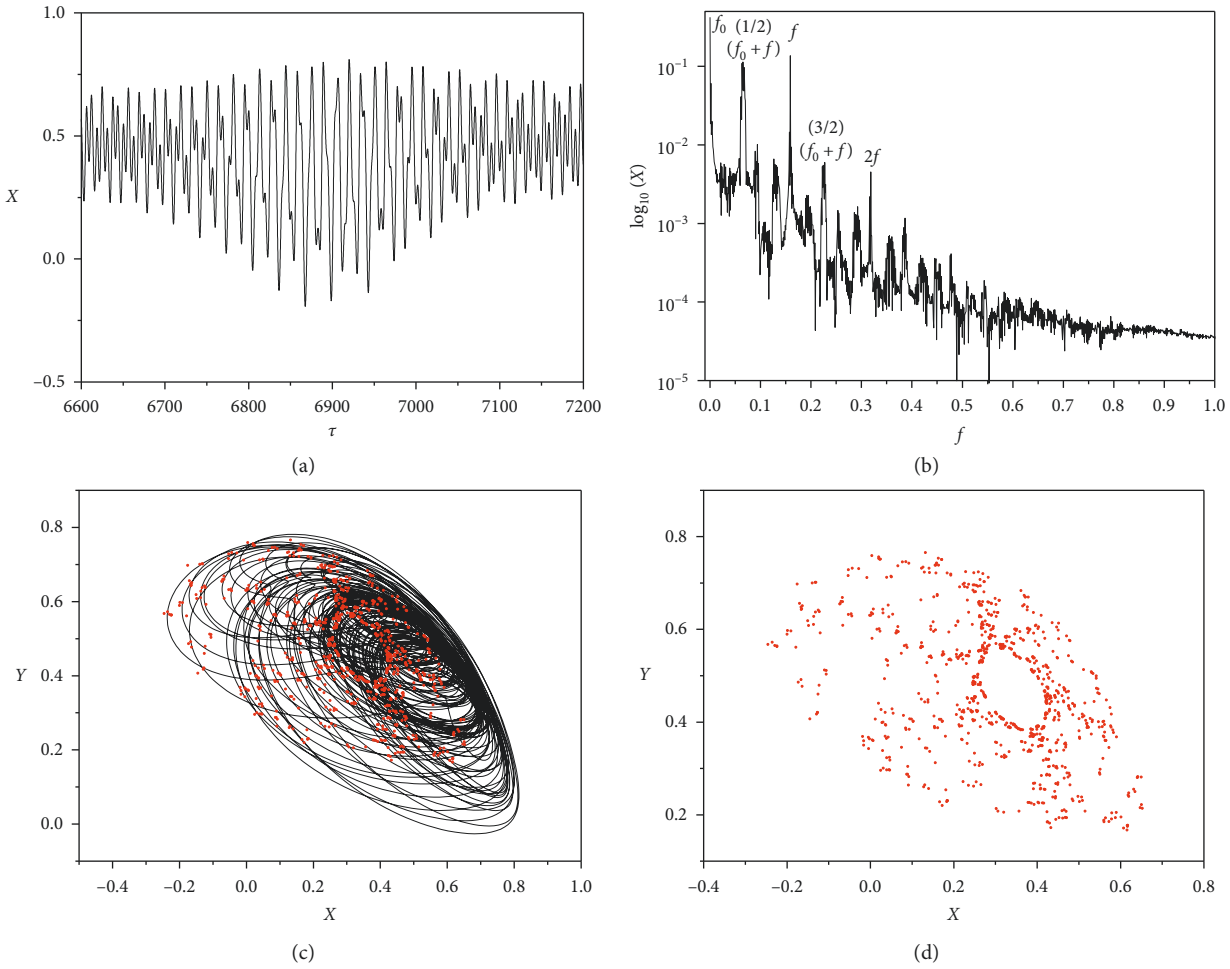

Figure 9: (a) Displacement. (b) Frequency response. (c) Rotor orbit. (d) Poincaré map where $\Omega_0 = 3.18$, $\eta = 100.58$, and $A_0 = 110$.

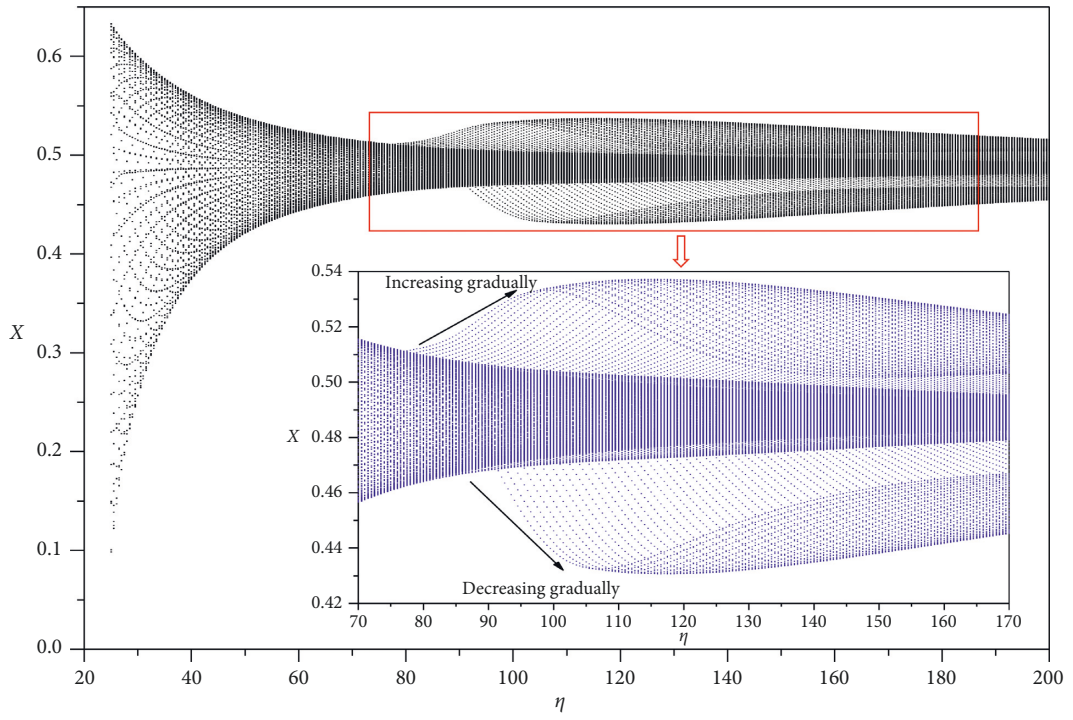

Figure 10: The bifurcation diagram of displacement X with frequency ratio η when $\Omega_0 = 2.12$ and $A_0 = 110$.

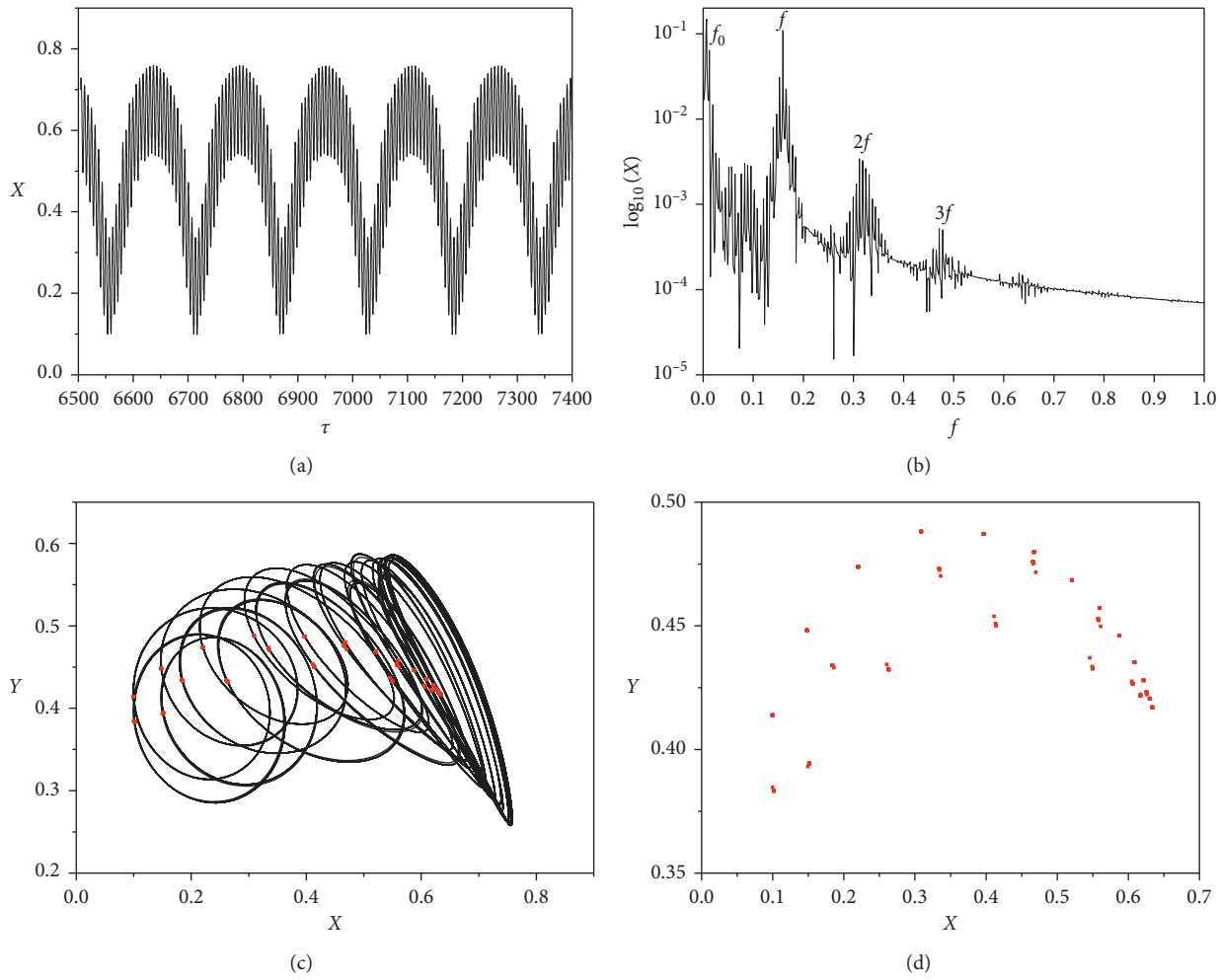

Figure 11: (a) Displacement. (b) Frequency response. (c) Rotor orbit. (d) Poincaré map where $\Omega_0 = 2.12$, $\eta = 25$, and $A_0 = 110$.

displacement of the rotor to increase continuously. Compared with the previous state, the displacement of the rotor has a significant variation. In the spectrogram, the power frequency f and its frequency multiplication components coexist; the frequency component f_0 still exists and continues to weaken. Meanwhile, the combined frequency component $(f + f_0)/2$ caused by nonlinear oil film force occurs; moreover, harmonic bifurcation phenomenon of the combined frequency appears which is affected by the heaving motion. The axis of the rotor is still a "band" ellipse, and its Poincaré map has a great change as a "tactile" shape. At this moment, the motion state of the system is more complex and appears as quasiperiodic characteristics.

Figure 14 is bifurcation diagram of the rotor displacement X attained by using heaving amplitude A_0 as control parameter where $\Omega_0 = 2.12$, $\eta = 100.58$, $\sigma = 3$, $\alpha = 0.1$, and $\lambda = 0.2$. It can be seen from the figure that the system has very rich dynamic characteristics, such as A_0 from 5 to 100; the displacement of the system under the action of nonlinear oil film force is gradually decreasing. At this point, the system exhibits a quasiperiodic motion state. As the amplitude increases further, the displacement of the rotor also undergoes a continuous increase process. This moment due to the increasingly severe heaving effect and the change of the oil film force caused by the heave motion, the displacement of the system has increased and the motion state is more complicated. Finally, the quasiperiodic motion transits to a chaotic state.

Figure 15 clearly shows the dynamic behaviors of the system at speed $\Omega_0 = 2.12$, frequency ratio $\eta = 100.58$, and amplitude $A_0 = 30$. The displacement of the system changes stably, except that the power frequency f and its multiplication component and the frequency component f_0 caused by the heaving motion still exist; moreover, the combined frequency component $(f + f_0)/2$ is small but has already appeared. The orbit of the rotor presents a regular ellipse, and its Poincaré map is a "spiral" attractor composed by discrete points. At this speed, the motion state of the system is a quasiperiodic state.

Figure 16 demonstrates the steady-state response of the system in which speed $\Omega_0 = 2.12$, frequency ratio $\eta = 100.58$, and amplitude $A_0 = 125$. As the amplitude of the heaving motion increases, the vertical displacement of the system begins to fluctuate. In addition to the previously occurring power frequency f and its multiplier component and the frequency component f_0 caused by the heave, the combined

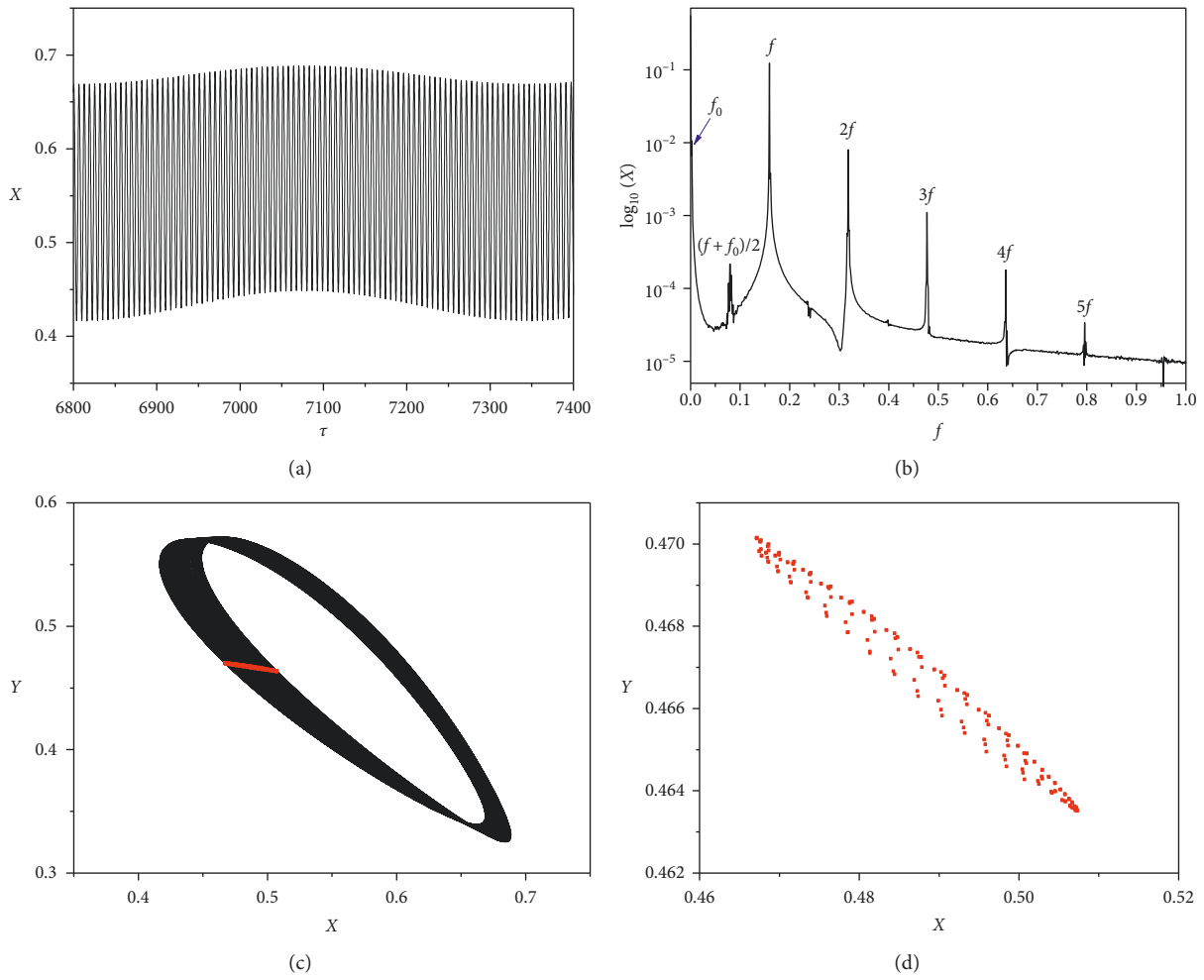

FIGURE 12: (a) Displacement. (b) Frequency response. (c) Rotor orbit. (d) Poincaré map where $\Omega_0 = 2.12$, $\eta = 85$, and $A_0 = 110$.

frequency component $(f+f_0)/2$ has obvious growth which indicates the motion of the system will become more complicated at this moment. The axis trajectory of the rotor is still a relatively regular elliptical "band," and its Poincaré map is an irregular set of discrete points. The system is in a quasiperiodic motion.

The steady-state response of the system at speed $\Omega_0 = 2.12$, frequency ratio $\eta = 100.58$, and amplitude $A_0 = 125$ is displayed in Figure 17. Except for the power frequency f and its multiplication component and the frequency component f_0, many odd-numbered frequency components of the combined frequency $(f+f_0)/2$ appear; meanwhile, harmonic components arise at each frequency peak. The trajectory of the rotor tends to be out of order, and its Poincaré map reflects irregular chaotic attractors. At this point, the system has entered a very complex and variable chaotic motion state.

4. Conclusion

The nonlinear dynamic characteristics of the marine rotor-bearing system are discussed in this article, in which the heaving motion of the ship is considered. The motion equation is solved by the Runge–Kutta method, and the conclusions obtained are as follows.

(1) The dynamic effect of the heaving motion on marine rotor system is derived from the inertial force, which engenders the vibrations of multifrequency responses and complex rotor trajectory. These performances reveal that the heave motion strongly affects the dynamic behaviors of the system.

(2) The dynamic characteristics of the rotor-bearing system are especially different under heaving motion. The path that the system enters chaos motion under heaving is period 1 ⟶ quasiperiod ⟶ period 2 ⟶ quasiperiod ⟶ chaos; however, the path the system enters chaos state without heaving is period 1 ⟶ period 2 ⟶ quasiperiod ⟶ chaos. It is obvious that the heaving motion gives the rotor system a new path into chaos.

(3) With the increase of the frequency ratio, the dynamics of the rotor system is the chaotic motion transition to quasiperiodic motion, whereas with the increase of the heaving amplitude, it is quasiperiodic motion to chaos. The effect of a smaller

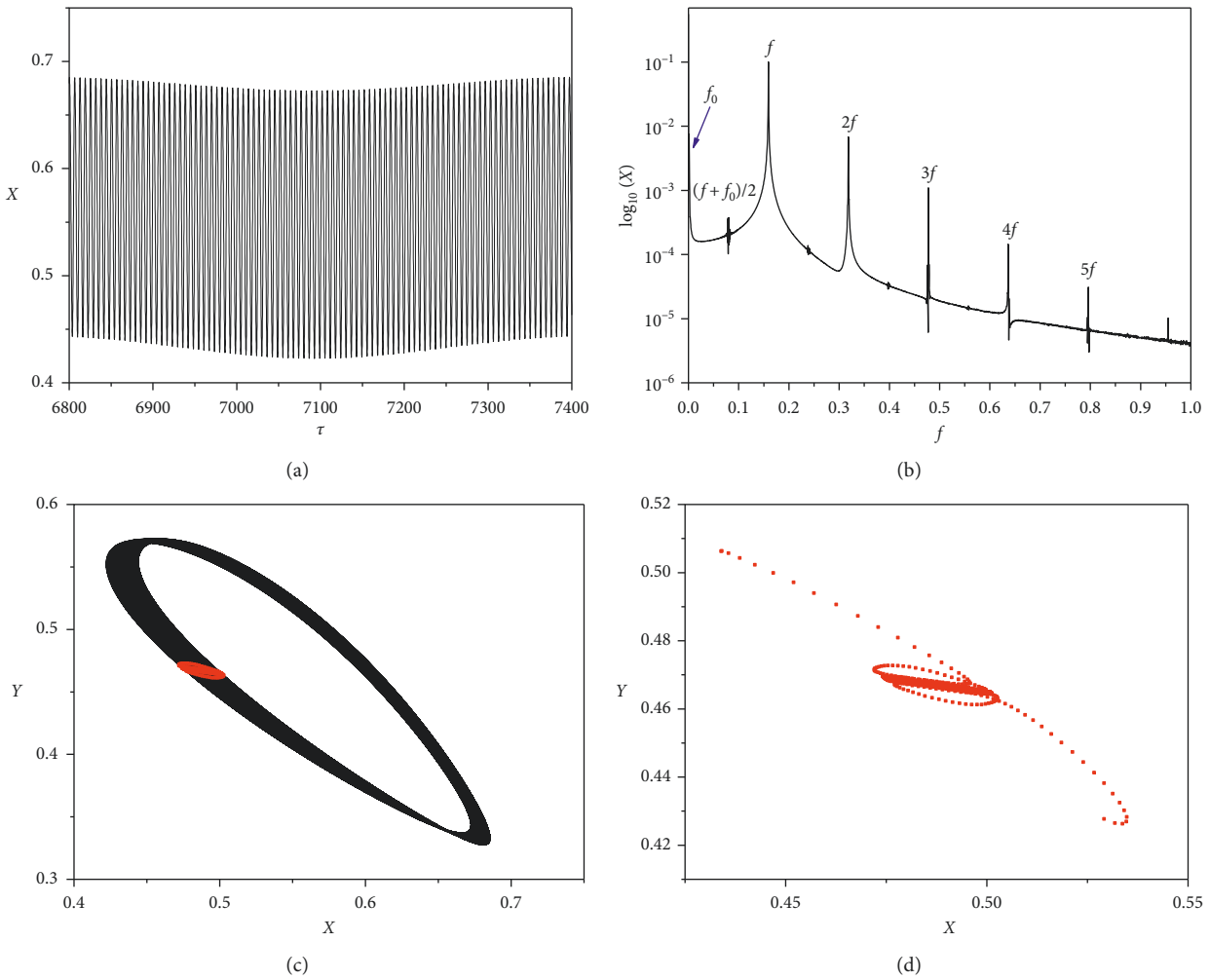

FIGURE 13: (a) Displacement. (b) Frequency response. (c) Rotor orbit. (d) Poincaré map where $\Omega_0 = 2.12$, $\eta = 105$, and $A_0 = 110$.

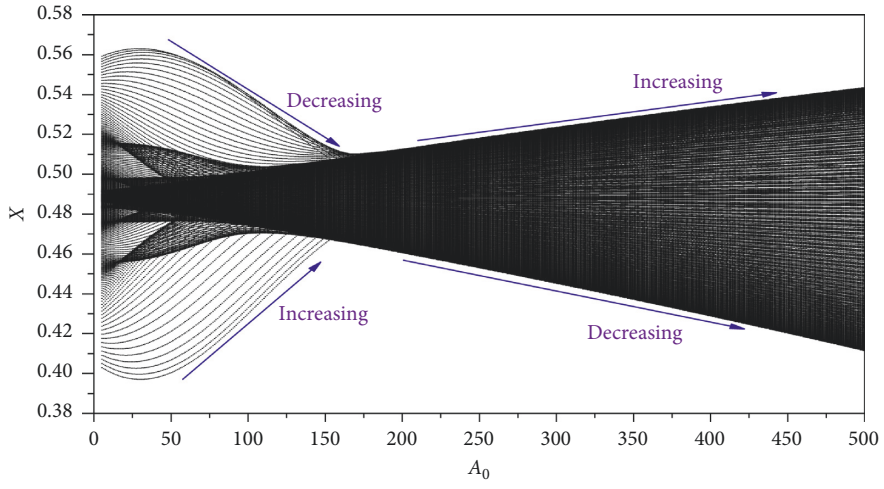

FIGURE 14: The bifurcation diagram of displacement X with amplitude A_0 when $\Omega_0 = 2.12$ and $\eta = 100.58$.

frequency ratio and a larger heave amplitude on the stable operation of the rotor system should be avoided.

This study is helpful for the engineers to recognize the influence of the heaving motion on the dynamic characteristics of the marine rotor-bearing system and its vibration control.

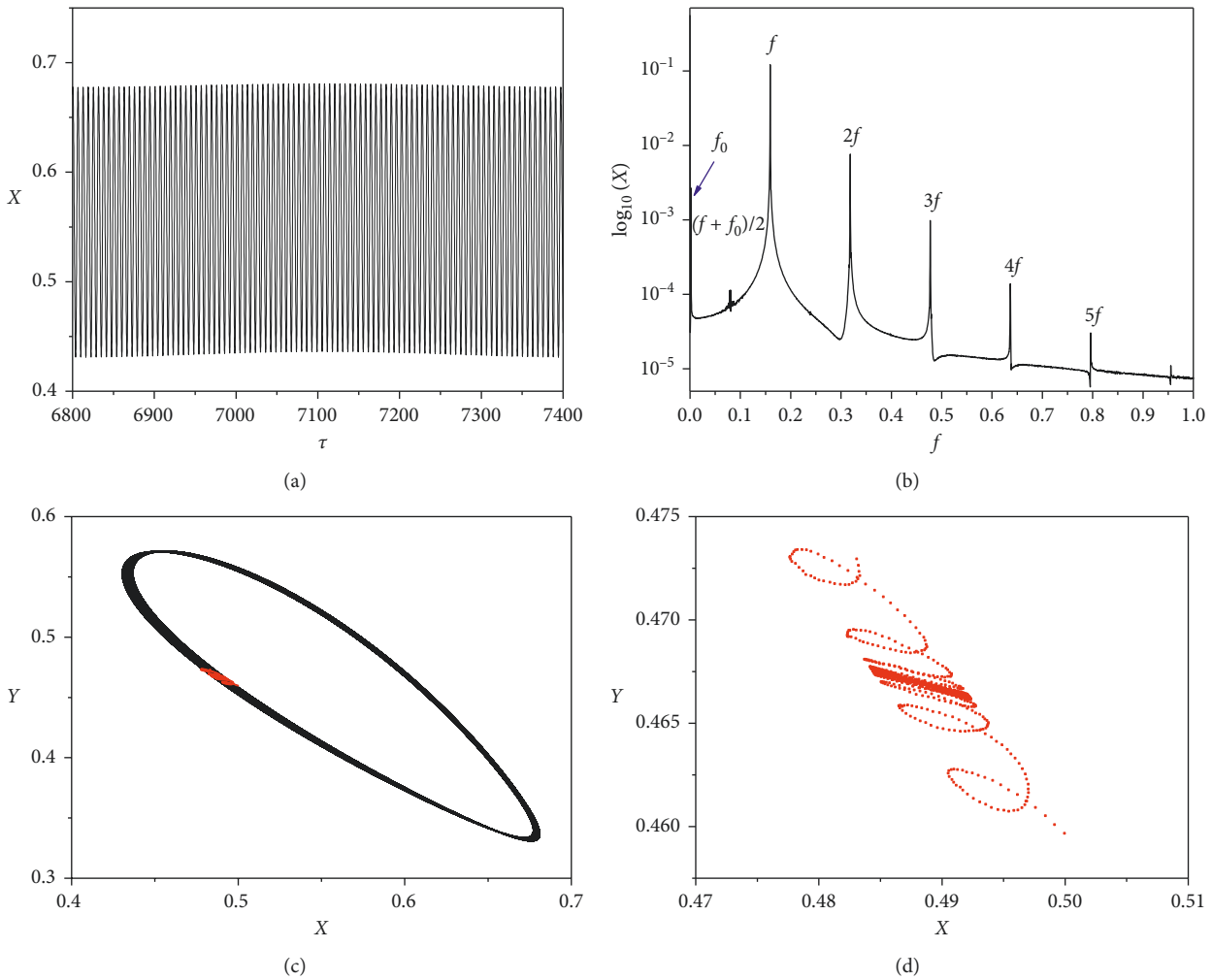

Figure 15: (a) Displacement. (b) Frequency response. (c) Rotor orbit. (d) Poincaré map where $\Omega_0 = 2.12$, $\eta = 100.58$, and $A_0 = 30$.

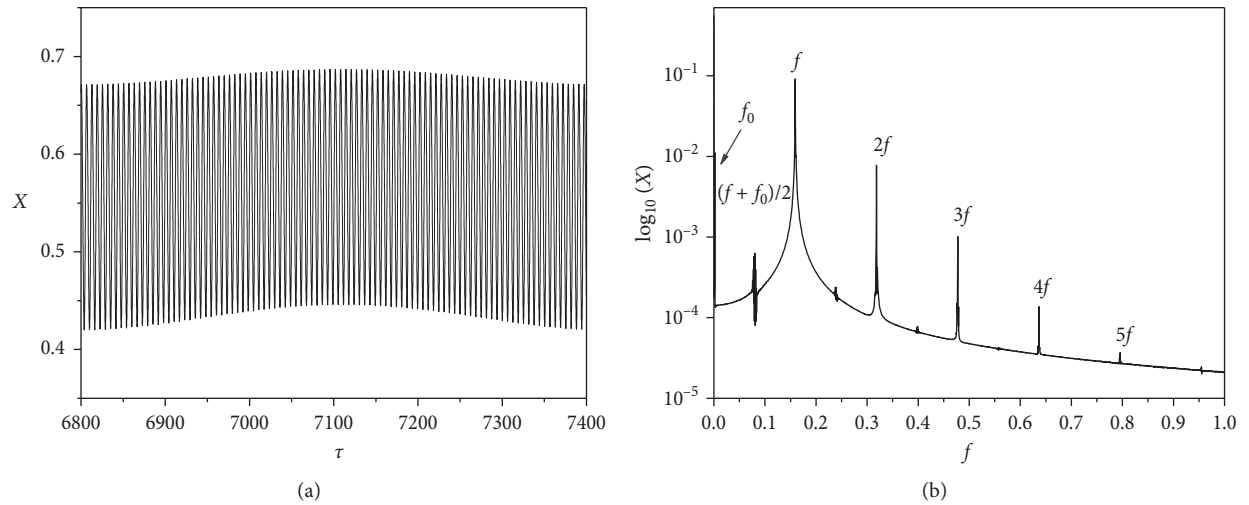

Figure 16: Continued.

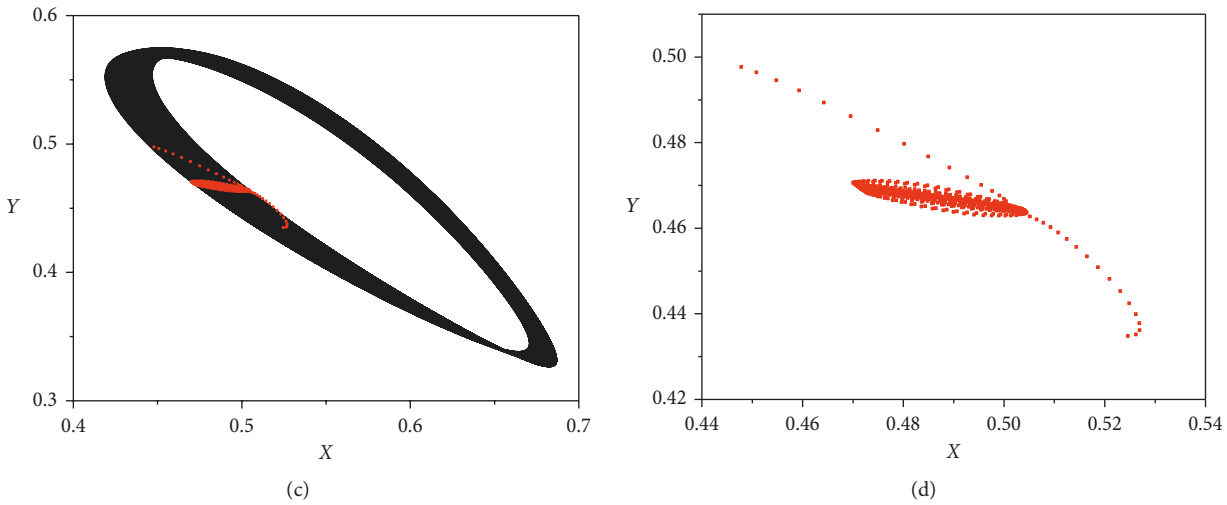

Figure 16: (a) Displacement. (b) Frequency response. (c) Rotor orbit. (d) Poincaré map where $\Omega_0 = 2.12$, $\eta = 100.58$, and $A_0 = 125$.

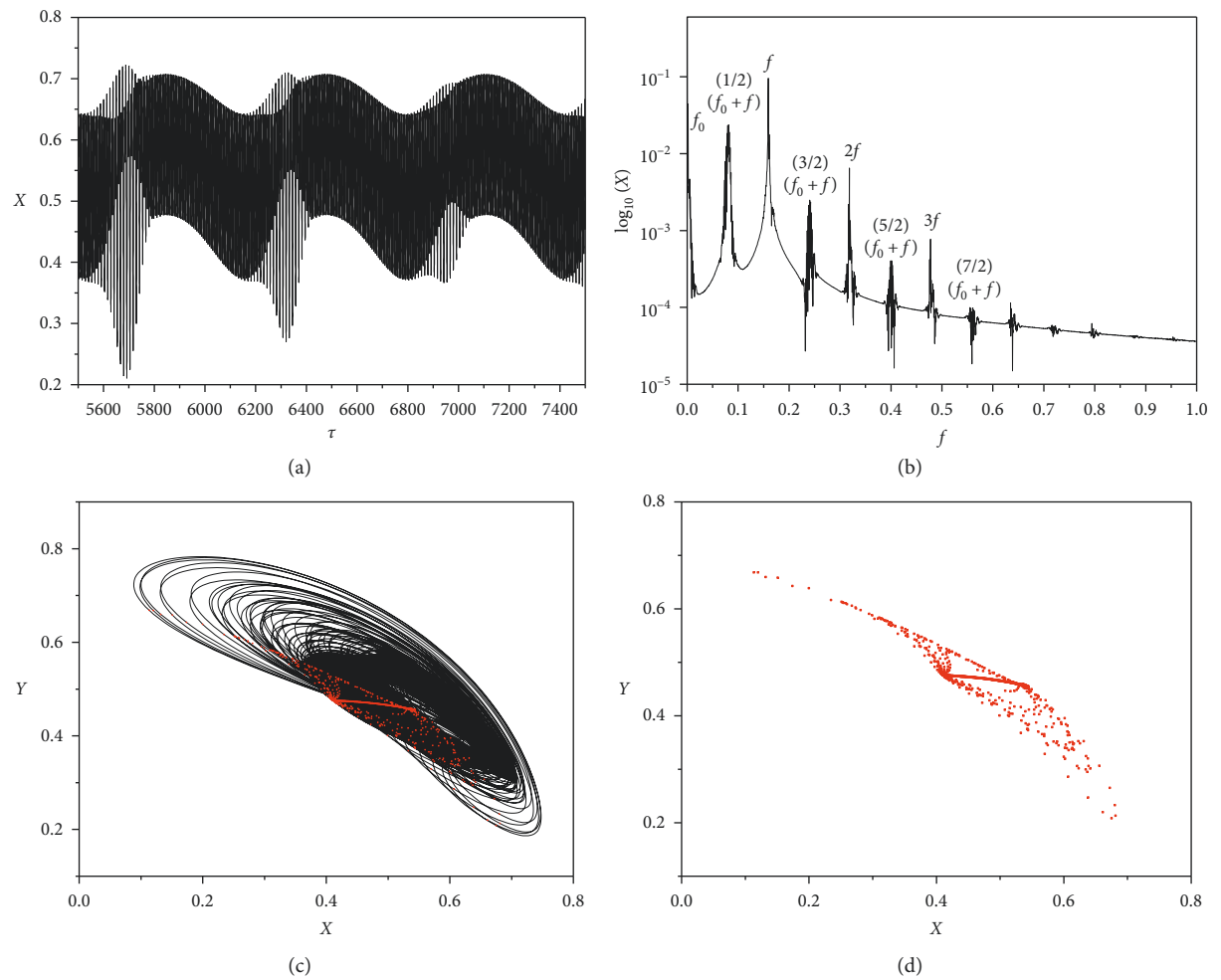

Figure 17: (a) Displacement. (b) Frequency response. (c) Rotor orbit. (d) Poincaré map where $\Omega_0 = 2.12$, $\eta = 100.58$, and $A_0 = 500$.

Notations

A_0: Amplitude of heaving motion
c: Bearing clearance
e: Eccentricity position of rotor center-line in journal bearing
f_x, f_y: Dimensionless oil film force of journal bearing
F_x, Oil film force of journal bearing
F_y:
g: The acceleration of gravity
h: The thickness of bearing oil film
m: The mass of disc
p: Oil film pressure
t: Time
x, y: Coordinates of the centers of disk
θ: Angle of the journal equilibrium position.
α: Dimensionless eccentricity
ε: The eccentricity ratio of bolster bearing
η : Dimensionless frequency ratio
φ: Circumferential azimuth of journal bearing
σ: Sommerfeld of bearing
λ: The ratio of length diameter
τ: Dimensionless time
Ω_0: Dimensionless rotor speed
ω: Rotor speed

Subscripts

0: Ship motion

Superscripts

$\dot{}$, $\ddot{}$: The first- and second-order derivatives with respect to time t
$'$, $''$: The first- and second-order derivatives with respect to dimensionless time τ.

Data Availability

The data used to support the findings of this study are available from the corresponding author upon request.

Conflicts of Interest

The authors declare that there are no conflicts of interest regarding the publication of this paper.

Acknowledgments

This work was supported by the National Natural Science Foundation of China (Grant no. 11372245) and the Natural Science Foundation of Shaanxi Province, China (Grant no. 2018JZ1001). This support is gratefully acknowledged.

References

[1] Y. Yu, Y. R. Hu, and X. D. Jin, "Current situation and trends in some aspects of research on nonlinear rolling of ships in waves," *Journal of Ship Mechanics*, vol. 34, no. 1, pp. 73–77, 2000.

[2] H. D. Nelson and W. L. Meacham, "Transient analysis of rotor-bearing systems using component mode synthesis," in *Proceedings of ASME 1981 International Gas Turbine Conference and Products Show*, vol. 41, Houston, TX, USA, March 1981.

[3] F. S. Lin, G. Meng, and E. Hahn, "Nonlinear dynamics of a cracked rotor in a maneuvering aircraft," *Applied Mathematics and Mechanics*, vol. 25, no. 10, pp. 1139–1150, 2004.

[4] H. Cho, H. Ryu, S. J. Shin, I.-J. Cho, and J.-S. Jang, "Development of a coupled analysis regarding the rotor/dynamic components of a rotorcraft," *Journal of Mechanical Science and Technology*, vol. 28, no. 12, pp. 4841–4856, 2014.

[5] K. Zheng, "Development of a coupled analysis regarding the rotor/dynamic components of a rotorcraft," in *Proceedings of 50th AIAA/ASME/SAE/ASEE Joint Propulsion Conference 2014*, Cleveland, OH, USA, July 2014.

[6] L. Hou, Y. S. Che, and Z. Y. Lu, "Bifurcation analysis for 2:1 and 3:1 super-harmonic resonances of an aircraft cracked rotor system due to maneuver load," *Nonlinear Dynamics*, vol. 81, no. 1-2, pp. 531–547, 2015.

[7] L. Hou and Y. S. Chen, "Dynamical simulation and load control of a Jeffcott rotor system in Herbst maneuvering flight," *Journal of Vibration and Control*, vol. 22, no. 2, pp. 412–425, 2016.

[8] R. Wang, X. Guo, and Y. Wang, "Nonlinear analysis of rotor system supported by oil lubricated bearings subjected to base movements," *Proceedings of the Institution of Mechanical Engineers, Part C: Journal of Mechanical Engineering Science*, vol. 230, no. 4, pp. 543–558, 2016.

[9] L. Wang, Y. Dai, and C. Yang, "Gust response analysis for helicopter rotors in the hover and forward flights," *Shock and Vibration*, vol. 2017, Article ID 8986217, 20 pages, 2017.

[10] S. Qin, Y. L. Zhang, and X. J. Chen, "Investigation of the nonlinear rolling of a ro-ro ship with slipping of heavy load," *Multibody System Dynamics*, vol. 14, no. 2, pp. 189–203, 2005.

[11] C. Holden, R. Galeazzi, C. Rodríguez et al., "Nonlinear container ship model for the study of parametric roll resonance," *Modeling, Identification and Control: A Norwegian Research Bulletin*, vol. 28, no. 4, pp. 87–103, 2007.

[12] C. D. Simonsen, J. F. Otzen, S. Joncquez, and F. Stern, "EFD and CFD for KCS heaving and pitching in regular head waves," *Journal of Marine Science and Technology*, vol. 18, no. 4, pp. 435–459, 2013.

[13] S. K. Lee, J. M. You, and H. H. Lee, "Experimental study on the six degree-of-freedom motions of a damaged ship floating in regular waves," *IEEE Journal of Oceanic Engineering*, vol. 41, no. 1, pp. 40–49, 2016.

[14] L. Chen, J. Wang, Q. Han, and F. Chu, "Nonlinear dynamic modeling of a simple flexible rotor system subjected to time-variable base motions," *Journal of Sound and Vibration*, vol. 404, pp. 58–83, 2017.

[15] G. Zhang, S. Liu, Z. Cao, R. Ma, and Z. Liu, "Analytical model of self-acting journal bearing subjected to base excitation for marine engine system," *Proceedings of the Institution of Mechanical Engineers, Part M: Journal of Engineering for the Maritime Environment*, vol. 227, no. 2, pp. 194–207, 2012.

[16] G. H. Zhang, S. P. Liu, and R. X. Ma, "Nonlinear dynamic characteristics of journal bearing-rotor system considering the pitching and rolling motion for marine turbo machinery," *Proceedings of the Institution of Mechanical Engineers, Part M: Journal of Engineering for the Maritime Environment*, vol. 229, no. 1, pp. 95–107, 2013.

[17] W. Zhao, M. Li, and L. Xiao, "Nonlinear dynamic behaviors of a marine rotor-bearing system coupled with air bag and floating-raft," *Shock and Vibration*, vol. 2015, Article ID 620968, 18 pages, 2015.